Dissecting Response to Cancer Immunotherapy by Applying Bayesian Network Analysis to Flow Cytometry Data

Short title: Bayesian network analysis of immune signaling networks FACS data

Andrei S. Rodin[*1], Grigoriy Gogoshin[1], Lei Wang[2], Colt Egelston[2], Russell C. Rockne[1], Joseph Chao[3], Peter P. Lee[*2]

* Corresponding authors

[1] Department of Computational and Quantitative Medicine

Beckman Research Institute

City of Hope National Medical Center

1500 East Duarte Road

Duarte, CA 91010 USA

[2] Department of Immuno-Oncology

Beckman Research Institute

City of Hope National Medical Center

1500 East Duarte Road

Duarte, CA 91010 USA

[3] Department of Medical Oncology & Therapeutics Research

City of Hope National Medical Center

1500 East Duarte Road

Duarte, CA 91010 USA

Authors / contributions

Andrei S. Rodin

https://orcid.org/0000-0002-2570-0332

Department of Computational and Quantitative Medicine

Beckman Research Institute

City of Hope National Medical Center

1500 East Duarte Road

Duarte, CA 91010 USA

arodin@coh.org

626-218-3807

Contributor role: Conceptualization, formal analysis, funding acquisition, investigation, methodology, project administration, resources, supervision, visualization, writing (original draft preparation).

Grigoriy Gogoshin

Department of Computational and Quantitative Medicine

Beckman Research Institute

City of Hope National Medical Center

1500 East Duarte Road

Duarte, CA 91010 USA

Contributor role: Conceptualization, data curation, formal analysis, investigation, methodology, software, visualization, writing (original draft preparation).

Lei Wang

Department of Immuno-Oncology

Beckman Research Institute

City of Hope National Medical Center

1500 East Duarte Road

Duarte, CA 91010 USA

Contributor role: Conceptualization, data curation, formal analysis, investigation, methodology, writing (original draft preparation).

Colt Egelston

Department of Immuno-Oncology

Beckman Research Institute

City of Hope National Medical Center

1500 East Duarte Road

Duarte, CA 91010 USA

Contributor role: Conceptualization, data curation, formal analysis, investigation, methodology.

Russell C. Rockne

https://orcid.org/0000-0002-1557-159X

Department of Computational and Quantitative Medicine

Beckman Research Institute

City of Hope National Medical Center

1500 East Duarte Road

Duarte, CA 91010 USA

Contributor role: Conceptualization, funding acquisition, methodology, visualization, writing (review and editing).

Joseph Chao

Department of Medical Oncology & Therapeutics Research

City of Hope National Medical Center

1500 East Duarte Road

Duarte, CA 91010 USA

Contributor role: Conceptualization, data curation, funding acquisition, investigation, project administration, resources, writing (review and editing).

Peter P. Lee

https://orcid.org/0000-0002-2660-4377

Department of Immuno-Oncology

Beckman Research Institute

City of Hope National Medical Center

1500 East Duarte Road

Duarte, CA 91010 USA

plee@coh.org

626-506-5585

Contributor role: Conceptualization, funding acquisition, investigation, methodology, project administration, resources, supervision, visualization, writing (original draft preparation).

Abstract

Cancer immunotherapy, specifically immune checkpoint blockade therapy, has been found to be effective in the treatment of metastatic cancers. However, only a subset of patients with certain cancer types achieve clinical responses. Consequently, elucidating immune system-related pre-treatment biomarkers that are predictive with respect to sustained clinical response is a major research priority. Another research priority is evaluating changes in the immune system before and after treatment in responders and non-responders. Specifically, our group has been studying immune signaling networks as an accurate reflection of the global immune state. Flow cytometry data (FACS, Fluorescence-activated cell sorting) characterizing immune signaling in peripheral blood mononuclear cells (PBMC) from gastroesophageal adenocarcinoma (GEA) patients were used to analyze changes in immune signaling networks in this setting. We developed a novel computational pipeline to perform secondary analyses of FACS data using systems biology / machine learning / information-theoretic techniques and concepts, primarily based on Bayesian network modeling. Application of this novel pipeline resulted in determination of immune markers, combinations / interactions thereof, and corresponding immune cell population types that are associated with clinical responses. Future studies are planned to generalize our analytical approach to different cancer types and corresponding datasets.

Author Summary

It is difficult to predict whether a cancer patient undergoing immunotherapy treatments will respond. As immunotherapy is expensive and may lead to autoimmune toxicities, patient selection is an important issue. One way to gain deeper insight into the underlying processes is to study changes in immune signaling networks during the treatment course. These networks can be modeled, visualized, and quantified using systems biology / machine learning methods, such as Bayesian networks (BNs). Here, we present a BN-based analytical strategy for devising and comparing immune signaling networks, and apply it to data obtained from patients in a gastrointestinal cancer immunotherapy clinical trial. We identify potentially predictive immune biomarkers, and compare and contrast the resulting network models in different groups of patients, before and after therapy. Our analytical strategy generalizes to different cancers and immunotherapy regimens.

Introduction

Automated analysis of high-dimensional cytometry data is an active bioinformatics research area [1,2]. Increasingly more sophisticated approaches, mostly of the data mining / machine learning variety, have recently been proposed for the primary analysis of such data [3,4,5,6,7]. However, emphasis remains on *primary* data analysis, which is largely reduced to automated gating, clustering, visualization and, subsequently and optionally, cellular identity / population type assignment [8,9]. Identification of clinically useful markers (and, perhaps even more importantly, marker combinations) is a *secondary* data analysis task, belonging to the realm of systems biology. To the best of our knowledge, there is currently no systems biology data analysis pipeline aimed specifically at high-dimensional data (including cytometry) in the immuno-oncology domain [10,11,12,13]. For example, recent works in the field [14,15,16,17,18] reduce the markers' deduction to classification and either semi-manual or pairwise combinatorics. Although these analyses are elegant and valid, their completeness and generalizability is suboptimal. Notably, such analyses are deficient in automatically assessing higher-order marker interactions. This is where network-based approaches, such as Bayesian network (BN) modeling, may be useful. To the best of our knowledge, there has been only one flow cytometry dataset (RAF signaling pathway) subjected to the BN treatment to-date [19,20,21,22,23]. While valuable as a proof-of-concept [19,20], and as a useful platform for further BN methodology development [21,22,23], it did not lead to wider acceptance of the BN methodology in the field. In this study, we introduce a comprehensive BN-centered analysis strategy aimed at the FACS (fluorescence-activated cell sorting) data analysis in the immuno-oncology context. As a part of this strategy, we introduce a novel technique, based on the "indicator/contrast variable", for comparing similar but distinct BNs (such as generated in responders vs. non-responders, before vs. after treatment, etc.)

Gastroesophageal adenocarcinomas (GEA) comprised of both stomach and esophageal cancers in aggregate account for a large proportion of global cancer-related mortality [24]. In addition to surgery, chemotherapy,

radiotherapy, and targeted therapy, immunotherapies such as immune checkpoint blockade (ICB) can serve as promising treatment options for GEA patients. However, the current response rate to ICB in such patients is still very low, with objective response rates less than 20% in all-comers [25]. Therefore, it is critical to identify biomarkers that can effectively predict clinical response to ICB in a subset of patients.

Currently, reliable predictive ICB biomarkers for GEA outside of genomic microsatellite instability (MSI) and Epstein-Barr virus (EBV) detection remain very limited; such potential predictive biomarkers can be identified based on the systemic immunological features that can be measured by using peripheral blood immune cells from GEA patients.

In our studies, we have collected peripheral blood mononuclear cell (PBMC) samples from metastatic GEA patients receiving anti-PD-1 (Pembrolizumab) along with radiation therapy. Three immune signaling flow cytometry panels (Adaptive, Checkpoint, Immune) were generated from each sample (see *Materials and Methods: Flow Cytometry* for detailed panel description), comprising the bulk of our FACS data. Importantly, we had PBMC samples from patients at baseline before the therapy (day 1) and after therapy (day 21). As a result, immunological changes in PBMC samples could be correlated to clinical response to immunotherapy in these patients.

Results

Basic computational pipeline, and baseline immune signaling FACS panels analyses

Our basic computational pipeline consists of (1) discretizing FACS measurements into 2-8 bins using maximum entropy, (2) performing full BN analysis (i.e., reconstructing the complete BN) for one FACS panel, clinical response status variable, and other available variables using our BN modeling software (BNOmics, see *Materials and Methods: Bayesian networks modeling* for details), (3) isolating a Markov blanket/ neighborhood (MN) of the response status variable, (4) analyzing the interplay of (usually no more than 4-8) immune system-related markers within the MN, (5) generating a compact set of rules for predicting response status from the markers' values, and (6) associating these rules with immune cell population subtypes. Afterwards, results obtained at different immunotherapy timepoints can be compared and contrasted (which is described in the next section, "contrast" analyses).

Three types of immune signaling FACS panels were analyzed, Checkpoint, Innate and Adaptive, with 14 immune markers in each. We will first illustrate the pipeline on the example of Checkpoint immune signaling FACS panel in GEA patients. The data contained 14 relevant PBMC immune marker variables measured (at day 1, before therapy, and day 21, after therapy) in 13 patients undergoing immunotherapy. Four patients exhibited significant (< -25% radius) tumor shrinkage and were labeled responders, with remaining nine labeled non-responders. All 13 patients were pooled together into a single dataset, and the complete dataset was used for the maximum entropy - based (three bins) discretization.

(Regarding clinical response definition: Our analytical strategy, specifically the BN reconstruction, is sufficiently robust with respect to the different algorithmic parameters. For instance, discretizing immune system marker FACS measurements into different number of bins (2-8) typically does not significantly alter the BN topology, or response status variable's MN composition. However, the analysis is

predictably sensitive to the varying assignment of the patients to the responder/non-responder categories. Our primary response data is before/after treatment change in tumor radius. There are three ways to discretize that into the response status. First, use purely data-driven, objective, criteria, such as maximum entropy (as was done in the above example, resulting in four responders and nine non-responders). Second, use a pre-specified clinical cutoff (with the patients showing < -25% tumor radius change classified as responders, which coincided perfectly with the aforementioned 4-9 split). Third, visualize the distribution function, with the goal of finding the notable inflection points. There are convincing rationales, both clinical/biological and theoretical, behind all three.)

Figure 1 depicts the full reconstructed Checkpoint immune signaling BN at day 1 (pre-treatment). The response status variable is designated “Tsize”, for “tumor size change”, in the graph. It is clear from the network that response status is directly strongly linked with five markers (TIGIT, CD4, CD8, CD160, 4-1BB, designated by dark grey nodes in the network) and, less strongly, with six other markers (TIM3, CD45RA, OX40, CXCR5, KLRG1, LAG3, light grey nodes in the network). Because the edges connecting Tsize to the latter six are, on average, significantly weaker than the edges between the latter six and the former five, we will only consider the former five markers as potential predictors of response to therapy. For example, although there is a direct edge between Tsize and CXCR5, it is very weak compared to the Tsize --- CD4 and CD4 --- CXCR5 edges, and so we conclude that the Tsize --- CXCR5 edge is likely an artifact of the very strong CD4 --- CXCR5 dependence.

Figure 1 legend: A full BN constructed from FACS data (Checkpoint immune signaling network panel) from 13 patients pre-immunotherapy treatment (day 1). Number next to the edge and edge thickness indicate dependency strength. (Arrows / edge directionality are for mathematical convenience only, to distinguish parent/offspring relationships during the BN reconstruction, and do not necessarily imply causation flow.) “Tsize” node is the response status variable (4 responders, 9 non-responders). Remaining nodes are immune marker variables. See text for further details.

Recall that the five variables directly influencing response status (TIGIT, CD4, CD8, CD160, 4-1BB) were discretized into three bins, “low”, “medium”, and “high”. Therefore, there are 3^5 = 243 possible configurations for these five variables. This is much better than the 3^14 ~= 4.8 million configurations in the full dataset before BN-derived dimensionality reduction, but still not feasible for the configuration-by-configuration manual scrutiny. However, we can rank these 243 configurations in order of decreasing frequency in the dataset (which indirectly map to the cell population types, from most to least frequent), and select a few most frequent configurations (using prespecified, or frequency distribution shape-driven, cutoffs). Then, we can re-sort them in order of decreasing probability of clinical response (tumor shrinkage) given the configuration. We illustrate this approach in Table 1 by showing 15 most frequent configurations, in order of decreasing probability of response --- meaning that responsive patients are associated with higher than randomly expected frequency of top-ranking configurations; these configurations might roughly correspond to particular cell population types. (The actual number of configurations, 15, was suggested by the shape of the configuration frequency function --- there is a noticeable dropoff (~0.02 to ~0.017) between the 15th and 16th configurations; the next noticeable dropoff is between the 35th and 36th configurations, and we have chosen the 15 configurations cutoff for presentation compactness).

Table 1. 15 most frequent predictive immune marker configurations (Checkpoint FACS panel), in descending order of probability of response. First column shows predictive immune marker configurations obtained from the MN of the response status variable, five markers in total (TIGIT, CD4, CD8, CD160, 4-1BB). “0”, “1”, “2” in the first column indicate “low”, “medium” and “high” values after discretization *via* maximum entropy. Second column shows configuration frequency; third column – probability of response.

Immune marker configuration	Configuration frequency	Probability of response
[0 1 2 2 2]	0.025596521	0.43048769
[2 1 2 2 2]	0.025189224	0.407215793
[2 2 1 2 2]	0.032789868	0.370882603
[2 2 2 1 2]	0.044319035	0.365182323
[1 1 2 2 2]	0.026780282	0.357207424
[2 2 2 1 1]	0.025560411	0.337571524
[2 2 2 2 2]	0.034634099	0.265528529
[1 2 2 2 2]	0.033621003	0.19072734
[0 2 2 2 2]	0.034101931	0.180530743
[0 0 1 0 0]	0.019338804	0.038043478
[0 0 0 1 0]	0.030720505	0.008510415
[0 0 0 0 0]	0.064393554	0.007913435
[0 0 0 0 1]	0.019329525	0.006856749
[1 0 0 1 0]	0.019939763	0.006141052
[1 0 0 0 0]	0.033787633	0.005642195

As summarized in Table 1, the analysis results are now compact enough to allow “manual” scrutiny. Note that the above process is completely automated --- the only two adjustable parameters are (1) the number of the potentially predictive variables to be selected from the MN of the response status variable, and (2) the number of the most frequent marker configurations. In the above example, the data itself suggested 5 and 15, respectively.

The above strategy (sorting first by frequency, then by response probability) favors the signals associated with more frequent marker combinations. Alternatively, one can sort by response probability only. Marker combinations associated with very high (or very low) response probabilities are likely to be less frequent. Such strategy is very similar to rare cells subsets discovery algorithms. In general, it is up to the investigator how the conditional probability tables are to be re-sorted once the list of potentially predictive variables is reduced to these inside the MN of response variable. The advantages of the “frequency-then-probability” sorting, as exemplified above, are two-fold: first, higher statistical robustness of discovered signals; second, a (typically) compact set of “rules” describing these signals.

By considering simultaneously the MN of the response variable (Figure 1), and the list of the most frequent marker configurations (Table 1), it is possible to elucidate a set of broad predictive patterns with respect to the clinical response variable. The most striking such pattern, clearly visible in the marker configuration list (Table 1), is a demarcation line between the top nine and the bottom six configurations. The former correspond to the higher response probability and show, on average, high marker concentrations (more “2”s across the board). The latter correspond to the low response probability and show lower marker concentrations (more “0”s across the board). In addition, Figure 1 suggests TIGIT (and, to a lesser extent, CD8) as the strongest individual predictor(s) of the clinical response. Indeed, when discretized into two bins using maximum entropy, high TIGIT values correspond to 0.28572 response probability, while low TIGIT values --- 0.051155 response probability.

Figure 2 depicts the BN generated from the same 13 patients using Innate immune signaling FACS panel. Out of 14 relevant immune markers, response status is directly strongly linked with eight markers (HLA-DR, PD-L1, CD3, CD20, CD83, CD1c, CD14, CD33, dark grey nodes in the network) and, less strongly, with one other marker (CD141, light grey node in the network).

Figure 2 legend: A full BN constructed from FACS data (Innate immune signaling network panel) from 13 patients pre-immunotherapy treatment (day 1). See Figure 1 legend for further details.

An 8-marker configuration frequency table is shown in Table 2. The actual number of configurations shown (20) was suggested by the shape of the configuration frequency function, which had the first noticeable dropoff at 20.

Table 2. 20 most frequent predictive immune marker configurations (Innate FACS panel), in descending order of probability of response. First column shows predictive immune marker configurations obtained from the MN of the response status variable, eight markers in total (HLA-DR, PD-L1, CD3, CD20, CD83, CD1c, CD14, CD33). “0”, “1”, “2” in the first column indicate “low”, “medium” and “high” values after discretization *via* maximum entropy. Second column shows configuration frequency; third column – probability of response.

Immune marker configuration	Configuration frequency	Probability of response
[2 1 0 1 2 1 2 2]	0.018250493	0.647765924
[2 2 2 1 2 2 1 0]	0.009584724	0.639289968
[2 1 1 1 2 1 2 2]	0.030847668	0.604122614
[2 2 2 1 2 2 1 1]	0.009815632	0.585641662
[2 1 1 2 2 1 2 2]	0.016348116	0.368976845
[2 2 2 2 2 2 2 2]	0.026929961	0.357136225
[1 2 2 2 1 2 1 0]	0.008111548	0.249001528
[1 2 2 2 1 2 1 1]	0.017652787	0.246288005
[2 1 2 1 2 1 0 2]	0.008588691	0.202118907
[2 2 2 2 2 1 2 2]	0.043024883	0.141053759
[2 2 2 2 2 1 1 2]	0.008973863	0.138153272
[1 2 2 2 1 2 0 0]	0.007996094	0.137888841
[1 2 2 2 1 2 0 1]	0.007768122	0.133538591
[0 0 0 0 0 0 1 0]	0.014749811	0.063120965
[0 0 0 0 0 0 1 1]	0.007439046	0.036651663
[0 0 0 0 0 0 0 1]	0.008566079	0.025902659

[0 0 0 0 1 0 0 0]	0.015771935	0.015205614
[0 0 0 0 0 0 0 0]	0.060293803	0.014164858
[0 0 0 0 0 0 2 1]	0.008461279	0.013066773
[1 0 0 0 0 0 0 0]	0.018650668	0.006697443

Similar to Table 1 (Checkpoint FACS panel), the most striking feature of the marker configuration list (Table 2) is a clear demarcation line between the top 13 and the bottom 7 configurations. The former correspond to the higher response probability and show, on average, high marker concentrations (more "2"s across the board). The latter correspond to the low response probability and show lower marker concentrations (more "0"s across the board). However, in contrast to the Checkpoint immune signaling network results, no particular markers (out of 8) stand out as the strongest individual predictors. In conclusion, on average, high values of HLA-DR, PD-L1, CD3, CD20, CD83, CD1c, CD14 and CD33 predict favorable response to immunotherapy.

Figure 3 depicts the BN generated from the same 13 patients using Adaptive immune signaling FACS panel. Out of 14 immune markers, response status is directly strongly linked with four markers (CXCR3, CCR4, CD8, CXCR5, dark grey nodes in the network) and, less strongly, with five other markers (CCR10, ICOS, CD73, CD4, CD45RA, light grey nodes in the network).

Figure 3 legend: A full BN constructed from FACS data (Adaptive immune signaling network panel) from 13 patients pre-immunotherapy treatment (day 1). See Figure 1 legend for further details.

A 4-marker configuration frequency table is shown in Table 3. The actual number of configurations shown (10) was suggested by the shape of the configuration frequency function, which had the first noticeable dropoff at 10.

Table 3. 10 most frequent predictive immune marker configurations (Adaptive FACS panel), in descending order of probability of response. First column shows predictive immune marker configurations obtained from the MN of the response status variable, four markers in total (CXCR3, CCR4, CD8, CXCR5). “0”, “1”, “2” in the first column indicate “low”, “medium” and “high” values after discretization *via* maximum entropy. Second column shows configuration frequency; third column – probability of response.

Immune marker configuration	Configuration frequency	Probability of response
[2 1 2 2]	0.035208137	0.40633172
[2 2 2 2]	0.152017497	0.377085493
[2 2 1 2]	0.04015162	0.347131651
[1 2 2 2]	0.038397874	0.226539338
[1 1 1 1]	0.040425037	0.08891941
[0 0 1 0]	0.035153813	0.038792148
[0 1 0 0]	0.037663102	0.018363657
[0 0 0 1]	0.04120894	0.008200336
[0 0 0 0]	0.124036248	0.007630638
[1 0 0 0]	0.028889777	0.00517798

Similar to the Tables 1 and 2, the top rows (higher probability of response) show, on average, high marker concentrations (more “2”s across the board), and the bottom rows (low probability of response) show lower marker concentrations (more “0”s across the board). Amusingly, the 5th row presents an almost perfect “borderline” case --- medium concentrations for all markers (all “1”s), and an intermediate probability of response (0.08891941). No particular markers (out of 4) stand out as the strongest individual predictors. In conclusion, on average, high values of CXCR3, CCR4, CD8 and CXCR5 predict favorable response to immunotherapy.

Separation into major immune cell types, and “contrast” (before/after immunotherapy, responders/non-responders) analyses in Checkpoint and Adaptive immune signaling networks.

In the above analyses, we have used all markers available on the corresponding FACS panels, with all immune cell types and subtypes pooled together. To achieve a higher analysis granularity, we have further separated each FACS dataset into four subsets, according to the four major immune cell types: (1) Naïve CD4, (2) Naïve CD8, (3) Non-naïve CD4, (4) Non-naïve CD8. These were stratified using CD4, CD8, CCR7 and CD45RA markers, according to the following membership rules: (1) 1011, (2) 0111, (3) 1010+1001+1000, (4) 0110+0101+0100, where “1” means high, and “0” – low marker concentration of CD4, CD8, CCR7 and CD45RA, in that order. The cutoff points between “high” and “low” were defined separately for the Checkpoint and Adaptive networks (due to different calibrations) and were as follows: Checkpoint: CD4=1500, CD8=750, CCR7=150, CD45RA=400; Adaptive: CD4=1000, CD8=1000, CCR7=150, CD45RA=1000.

Subsequently, we have generated BNs for 32 sub-datasets: (responders/non-responders) x (before/after immunotherapy) x (Checkpoint / Adaptive) x (Naïve CD4 / Naïve CD8 / Non-naïve CD4 / Non-naïve CD8). Markers CD4, CD8, CCR7 and CD45RA were naturally excluded from these networks. Comparisons of these networks allowed us to evaluate changes in immune signaling networks in

responders and non-responders before (day 1) and after (day 21) immunotherapy, stratified by a major immune cell type. In order to quantify and automate these comparisons, we have introduced "indicator/contrast variables", as illustrated in the following example (Checkpoint network, Non-naïve CD4 sub-dataset):

Figure 4 depicts four BNs obtained using 8-bin maximum entropy discretization --- (a) day 1, non-responders only, (b) day 1, responders, (c) day 21, non-responders, (d) day 21, responders.

Figure 4 legend: BNs constructed from FACS data (Checkpoint immune signaling network panel, Non-naïve CD4 sub-dataset) from 13 patients. (a) day 1, non-responders only, (b) day 1, responders, (c) day 21, non-responders, (d) day 21, responders. See Figure 1 legend for further details.

At this stage, it was unclear how to efficiently compare/contrast these networks in order to tease out the most significant changes, short of manually enumerating the topological differences. Therefore, we have introduced a "Contrast" variable with four distinct states (day 1 / non-response, day 1 / response, day 21 / non-response and day 21 / response) and included it in the pooled, or "supergraph" BN (Figure 5). In Figure 5, four markers (KLRG1, BTLA, OX40 and, to a lesser extent, PD-1) were observed in the MN of the "Contrast" variable, suggesting that it is the behavior of these four markers (reflected in the corresponding MNs in the original four stratified networks, Figure 4abcd) that differentiate the responder / non-responder / day 1 / day 21 states.

Figure 5 legend: A BN constructed from FACS data (Checkpoint immune signaling network panel, Non-naïve CD4 sub-dataset) from 13 patients. "Contrast" node is the indicator variable with four states, (day 1 / non-response, day 1 / response, day 21 / non-response and day 21 / response). See Figure 1 legend for further details.

To look even deeper, we have subsequently introduced two separate contrast variables ("Response" and "Day"), and constructed four contrast networks shown in Figure 6: (a) at day 1, responders vs. non-responders, (b) at day 21, responders vs. non-responders, (c) non-responders, at day 1 vs. day 21, and (d) responders, at day 1 vs. day 21.

Figure 6 legend: Contrast BNs constructed from FACS data (Checkpoint immune signaling network panel, Non-naïve CD4 sub-dataset) from 13 patients. (a) at day 1, responders vs. non-responders, (b) at day 21, responders vs. non-responders, (c) non-responders, at day 1 vs. day 21, and (d) responders, at day 1 vs. day 21. "Day" node is the indicator variable with two states (day 1, day 21). "Response" node is the indicator variable with two states (response, non-response). See Figure 1 legend for further details.

We were especially interested in Figure 6b that compares/contrasts responders and non-responders at day 21 (post-treatment). It appears that there is just one marker with a strong network edge in the MN of the "response" variable, KLRG1. By looking at KLRG1's MNs in the stratified networks (Figure 4cd), we conclude that the major difference between the Checkpoint network in responders and non-responders at day 21 (after immunotherapy treatment) is a relatively less prominent dependency (correlation) between KLRG1 and TIGIT, and an absence of dependency between KLRG1 and TIM3 in responders (compared to non-responders). This is an example of an interaction, and change thereof, that would have been exceedingly difficult to pinpoint without the BN comparison analysis along the above lines. In other words, our analytical strategy automatically identified the single most important topological difference between the immune signaling networks reflecting two different states (responders vs. non-responders after immunotherapy). (We need not, of course, concentrate on only the one top difference.)

The results of remaining seven sub-dataset analyses (that is, Adaptive immune signaling network panel x Non-naïve CD4 sub-dataset, and both Adaptive and Checkpoint panels x Naïve CD4, Naïve CD8 and Non-naïve CD8 sub-datasets) are shown in S1 Appendix (together with the itemized figure

captions/legends). To illustrate another case of a “contrast” network analysis, consider, for example, S1 Figure 52, which contrasts Adaptive Non-naïve CD8 networks at day 1 between responders and non-responders. The strongest network edge in the MN of the “response” variable points to ICOS, and after looking at the ICOS node’s MNs in the corresponding stratified networks (S1 Figure 46 - day 1, responders, and S1 Figure 47 - day 1, non-responders) we conclude that there are interactions (correlations, dependencies) between ICOS and other markers (notably, CD127) that are present in responders but not in non-responders. Again, just like in a previous example, we were able to automatically single out one strongest interaction (network edge, in this case between ICOS and CD127) that distinguishes between the two different network states.

The above analyses illustrate the process of identifying markers and also higher-order marker interactions that distinguish immune signaling networks in responders and non-responders before and after immunotherapy treatment. The more theoretical question remains --- does the “contrast variable” approach comprehensively capture the topology changes between the networks being compared? In a BN, a presence of an edge is nothing more than a presence of a node in the parent set of another node. Any time an edge is introduced, we are in fact looking at the corresponding change in the joint distribution of the two nodes in question: therefore, the “contrast” node is necessarily dependent on the joint distribution of the two nodes that gain or lose an edge. Consequently, appearance / disappearance of an edge A->B is reflected in that the contrast C gets “pulled in” as A&B -> C. This is because, in order for contrast C to be independent, we must have $P(C \mid A\&B) = P(C)$. However, $P(A\&B \mid C)\, P(C) = P(A\&B)\, P(C \mid A\&B)$, and so $P(C \mid A\&B) = P(A\&B \mid C)\, P(C) / P(A\&B)$. Thus, the only way C can be independent of A&B is if $P(A\&B \mid C) = P(A\&B)$, which we know is not true because it is given that $P(A\&B \mid C=0) \neq P(A\&B \mid C=1)$. Therefore, the variations that are not “detected” by contrast variable must be either noise or structural variants from the same BN equivalence class. Moreover, appearance/disappearance of an edge is not the only inter-BN difference that will be detected *via* contrast variables. For example, the same edge could represent a direct or an inverse relationship in two graphs, so one would not necessarily know

the difference by just looking at the edges, but it would be a distributional difference that would be captured by a contrast variable all the same. In fact, all differences associated with going from one graph to another are necessarily nothing but results of conditioning on the contrast variable in the supergraph --- for example, a non-response graph G0 (Figure 4c) is simply a supergraph G (Figure 6b) conditioned with contrast C (“Response”) = 0. Therefore, we can expect that all differences will necessarily be encapsulated by the contrast variable connectedness.

Discussion

In this study, we developed a novel secondary data analysis strategy aimed at FACS data in the immuno-oncology context. It is based on BN modeling, maximum entropy discretization, multi-stage marker configuration frequency sorting, and pooling sub-dataset BNs while introducing "contrast" variables. The end output of our computational pipeline consists of the following components: (a) a compact subset of potentially predictive (with respect to a clinical outcome or some other phenotype) markers, typically in the single digit (4-8) range, (b) a graphical causal model of the interactions between these predictors and other variables, together with the corresponding relative interaction strengths, (c) a compact list of the most frequent marker combinations, together with the corresponding outcome/phenotype probabilities, and (d) a shortlist of markers whose behavior (as reflected in their corresponding MNs in the stratified sub-networks) is significantly different between the varying immune signaling network states (responders / non-responders, before / after immunotherapy). These markers and combinations can subsequently be associated with the immune cell types/subtypes.

The main advantage of our novel analytical strategy is that it is fully automated and generalizable to other FACS datasets, of varying data structure and dimensionality. At the same time, it allows for certain amount of flexibility in the analysis process. First, different discretization approaches can be tried, depending on the investigators' understanding of what "high" and "low" might mean for a particular marker concentration. Second, more (or fewer) potential predictors can be selected from the outcome/phenotype variable's MN, depending on the BN's local sparseness and the general pattern of conditional independencies in the network. (This, however, is a complicated issue, and we plan to investigate it further as part of our ongoing BN methodological research.) Third, more (or fewer) potential predictor configurations (and corresponding cell types/subtypes) can be scrutinized at later analysis stages, depending, for example, on the size and coverage/purpose of the concrete FACS panel, or on

whether investigators are interested in rare cell types that are very strongly associated with particular outcomes/phenotypes.

There are two additional interrelated methodological caveats that are intrinsic to the BN modeling in general: dependency strength validation, and inter-network comparisons. Throughout this study, we use edge strengths to estimate statistical support for the networks and their features. Edge strength is conceptually similar to the marginal likelihood ratio test, in that it is proportional to the ratio of the BN model scoring function value when the edge is present in the BN to the BN model scoring function value when the edge is absent in the BN. Edge strengths do not directly translate into p-values; therefore, once a particular dependency/association is suggested by the BN, and is of interest to the investigators, one should follow up with a "traditional" statistical association test if a context-free p-value is desired. This said, edge strengths are directly comparable to each other within a single BN. However, it is not immediately clear whether they are directly comparable to each other *between* the BNs, even if the corresponding datasets are similar in their dimensionality. There are reasons to believe that edge strengths are linear functions of the dataset size (e.g., number of cells in one sample in the FACS context), but this aspect requires further investigation. For now, we would not necessarily advise comparing edge strengths between the networks (e.g., between Figures 1, 2, 3 in this study) unless the BN-generating datasets are very similar in their size and structure. Instead, when possible, the data should be pooled, and indicator/contrast variables (distinguishing the networks to be compared) introduced (e.g., Figures 5, 6 in this study).

In conclusion, since only some cancer patients tend to be responsive to ICB treatment, development of reliable predictive biomarkers for ICB treatment is urgently needed to select patients. While recent findings have shown some promise in tumor tissue-based immunological biomarkers [13], peripheral blood biomarkers are more accessible and less invasive [16]. In this study, peripheral blood FACS data, combined with our analytical strategy, have been successfully used to suggest such biomarkers, and gain

insight into their interactions and dynamics before and after treatment. In the future, we intend to generalize this approach to other cancer types, treatments, and patient cohorts.

Materials and Methods

Flow cytometry

Peripheral blood mononuclear cells (PBMCs) from patients consented to an IRB-approved protocol were isolated from heparinized blood by Ficoll-Paque density centrifugation and cryopreserved in 10% DMSO FBS. Cryopreserved PBMCs were thawed and stained with antibodies for the following flow cytometry panels:

Checkpoint panel: CD4, CD8, CD45RA, KLGR1, CCR7, CXCR5, 4-1BB, BTLA4, LAG3, OX40, CD160, TIGIT, PD1, TIM3;

Innate panel: CD3, CD14, CD16, CD20, CD33, CD56, CD11c, CD141, CD1c, CD123, CD83, HLA-DR, TCRgδ, PD-L1;

Adaptive panel: CD4, CD8, CCR10, CCR6, CD73, ICOS, CXCR3, CXCR5, CD45RA, CCR4, CCR7, CD25, CD127, PD1.

Flow cytometry was performed using Fortessa Flow Cytometers and flow cytometry data was analyzed using FlowJo software (BD Biosciences).

Bayesian networks modeling

BN modeling is a systems biology method that constructs a graphical visualization of a joint multivariate probability distribution of the random variables in the dataset. While recent BN modeling software implementations are highly scalable [26], combining scalability with mixed variable types (e.g., continuous and discrete) is less straightforward; an argument can be made [26,27] that adaptive discretization of continuous variables is a better solution, in practical terms, than imposing mixed distributional models. Therefore, in this study we were using full sample maximum entropy – based discretization which, among other things, allows us to adjust the under/over-fitting balance (i.e.,

specificity vs. sensitivity). Typically, discretizing into a smaller number of bins (2-3) increases sensitivity (higher edge density), and discretizing into a larger number of bins (4-8) increases specificity (lower edge density).

Detailed description of the BN methodology is outside the scope of this report; we refer the reader to [26] for the general description of BN modeling and our implementation thereof, and to [28] for a recent example application (to high-dimensional multimodal chromatin interaction data). However, certain important technical aspects need to be mentioned here, and are as follows: (1) edge directions in the BN do not necessarily indicate directionality of causation, but rather exist for the mathematical and computational convenience, to establish parent-offspring relationships, (2) in BN figures, numbers next to the edges and edge "thickness" specify relative edge strengths (which are marginal likelihood-based), (3) our BN implementation is based on a hybrid "sparse candidates" + "search-and-score" algorithm, and (4) when analyzing the reconstructed BNs, we often "zoom in" on the immediate Markov neighborhood (MN) of a specific variable (such as an immune system-related marker, or a patient's clinical response status), which corresponds to all the nodes (variables) directly linked to a specific variable in question. In fact, the central step in our computational analysis pipeline is using the full BN reconstruction to generate the MN for the clinical response status variable, and then assessing the interrelationships between the markers contained in that MN. (A caveat: MN is a simpler version of the Markov Blanket --- the latter takes into account parent-offspring relationship directionality --- meaning, for the practical purposes, that "two degrees of separation", or more, are sometimes needed for fully assessing the conditional independence relationships around a specific variable/node.)

Acknowledgements

The authors are grateful to Arthur D. Riggs and Sergio Branciamore for many stimulating discussions and useful suggestions.

Financial Disclosure Statement

This work was supported by the NCI Cancer Biology System Consortium U01CA23221601 grant (to P.P.L., R.C.R., and A.S.R.) and NIH NCI award P30CA033572. This work was also supported by the Susumu Ohno Chair in Theoretical and Computational Biology (held by A.S.R.), a Susumu Ohno Distinguished Investigator fellowship (to G.G.), and City of Hope funds (to G.G. and A.S.R.). This work was also partly supported by NIH grant 5K12CA001727-23 (to J.C.) and Merck Investigator Studies Program #52993 (to J.C.). The funders had no role in study design, data collection and analysis, decision to publish, or preparation of the manuscript.

Data Availability Statement

Principal datasets analyzed in this study have been deposited to Dryad (doi:10.5061/dryad.fxpnvx0ng).

https://doi.org/10.5061/dryad.fxpnvx0ng

All intermediate/auxiliary datasets will be made available by the authors, without undue reservation, to any qualified researcher.

Conflicts of Interest

J.C. has received research funding (institutional) and consultant/advisory fees from Merck and serves on the speaker's bureau for Merck.

References:

1. Mair F, Hartmann FJ, Mrdjen D, Tosevski V, Krieg C, Becher B. 2016. The end of gating? An introduction to automated analysis of high dimensional cytometry data. Eur J Immunol. 46(1):34-43. doi: 10.1002/eji.201545774. Epub 2015 Nov 30. Review. PMID: 26548301

2. Saeys Y, Van Gassen S, Lambrecht BN. 2016. Computational flow cytometry: helping to make sense of high-dimensional immunology data. Nat Rev Immunol. 20. 16(7):449-62. doi: 10.1038/nri.2016.56. Epub 2016 Jun 20. Review. PMID: 27320317

3. Gu Y, Zhang AC, Han Y, Li J, Chen C, Lo YH. 2019. Machine Learning Based Real-Time Image-Guided Cell Sorting and Classification Cytometry A. 95(5):499-509. doi: 10.1002/cyto.a.23764. Epub 2019 Apr 8. PMID: 30958640

4. Baron CS, Barve A, Muraro MJ, van der Linden R, Dharmadhikari G, Lyubimova A, de Koning EJP, van Oudenaarden A. 2019. Cell Type Purification by Single-Cell Transcriptome-Trained Sorting. Cell. 179(2):527-542.e19. doi: 10.1016/j.cell.2019.08.006.PMID: 31585086

5. Mazza EMC, Brummelman J, Alvisi G, Roberto A, De Paoli F, Zanon V, Colombo F, Roederer M, Lugli E. 2018. Background fluorescence and spreading error are major contributors of variability in high-dimensional flow cytometry data visualization by t-distributed stochastic neighboring embedding. Cytometry A. 93(8):785-792. doi: 10.1002/cyto.a.23566. Epub 2018 Aug 14

6. Yu JS, Pertusi DA, Adeniran AV, Tyo KEJ. 2017. CellSort: a support vector machine tool for optimizing fluorescence-activated cell sorting and reducing experimental effort. Bioinformatics. 15;33(6):909-916. doi: 0.1093/bioinformatics/btw710. PMID: 27998936

7. Pischel D, Buchbinder JH, Sundmacher K, Lavrik IN, Flassig RJ. 2018. A guide to automated apoptosis detection: How to make sense of imaging flow cytometry data. PLoS One. 13(5):e0197208. doi: 10.1371/journal.pone.0197208. eCollection 2018. PMID: 29768460

8. Nowicka M, Krieg C, Weber LM, Hartmann FJ, Guglietta S, Becher B, Levesque MP, Robinson MD. 2017. CyTOF workflow: differential discovery in high-throughput high-dimensional cytometry datasets. F1000Res. 6:748. doi: 10.12688/f1000research.11622.2. eCollection 2017. PMID: 28663787

9. Kimball AK, Oko LM, Bullock BL, Nemenoff RA, van Dyk LF, Clambey ET. 2018. A Beginner's Guide to Analyzing and Visualizing Mass Cytometry Data. J Immunol. 200(1):3-22. doi: 10.4049/jimmunol.1701494. PMID: 29255085

10. Palit S, Heuser C, de Almeida GP, Theis FJ, Zielinski CE. 2019. Meeting the Challenges of High-Dimensional Single-Cell Data Analysis in Immunology. Front Immunol. 10:1515. doi: 10.3389/fimmu.2019.01515. eCollection 2019. Review. PMID: 31354705;

11. Mair F, Tyznik AJ. 2019. High-Dimensional Immunophenotyping with Fluorescence-Based Cytometry: A Practical Guidebook. Methods Mol Biol. 2032:1-29. doi: 10.1007/978-1-4939-9650-6_1.PMID: 31522410

12. Guidelines for the use of flow cytometry and cell sorting in immunological studies (second edition). Eur J Immunol. 2019. 49(10):1457-1973. doi: 10.1002/eji.201970107. PMID: 31633216

13. Nishino M, Ramaiya NH, Hatabu H, Hodi FS. 2017. Monitoring immune-checkpoint blockade: response evaluation and biomarker development. Nat Rev Clin Oncol. 14(11):655-668. doi: 10.1038/nrclinonc.2017.88. Epub 2017 Jun 27. Review. PMID: 28653677).

14. Torang A, Gupta P, Klinke DJ 2nd. 2019. An elastic-net logistic regression approach to generate classifiers and gene signatures for types of immune cells and T helper cell subsets. BMC Bioinformatics. 20(1):433. doi: 10.1186/s12859-019-2994-z. PMID: 31438843

15. Leiserson MDM, Syrgkanis V, Gilson A, Dudik M, Gillett S, Chayes J, Borgs C, Bajorin DF, Rosenberg JE, Funt S, Snyder A, Mackey L. 2018. A multifactorial model of T cell expansion and durable clinical benefit in response to a PD-L1 inhibitor. PLoS One. 13(12):e0208422. doi: 10.1371/journal.pone.0208422. eCollection 2018. PMID: 30596661

16. Krieg C, Nowicka M, Guglietta S, Schindler S, Hartmann FJ, Weber LM, Dummer R, Robinson MD, Levesque MP, Becher B. 2018. High-dimensional single-cell analysis predicts response to anti-PD-1 immunotherapy. Nat Med. 24(2):144-153. doi: 10.1038/nm.4466. Epub 2018 Jan 8. Erratum in: Nat Med. 2018 Jul 2; PMID: 29309059

17. Auslander N, Zhang G, Lee JS, Frederick DT, Miao B, Moll T, Tian T, Wei Z, Madan S, Sullivan RJ, Boland G, Flaherty K, Herlyn M, Ruppin E. 2018. Robust prediction of response to immune checkpoint blockade therapy in metastatic melanoma. Nat Med. 24(10):1545-1549. doi: 10.1038/s41591-018-0157-9. Epub 2018 Aug 20. PMID: 30127394

18. Wistuba-Hamprecht K, Martens A, Weide B, Teng KW, Zelba H, Guffart E, Chen J, Garbe C, Newell EW, Larbi A, Pawelec G. 2017. Establishing High Dimensional Immune Signatures from Peripheral

Blood via Mass Cytometry in a Discovery Cohort of Stage IV Melanoma Patients. J Immunol. 198(2):927-936. doi: 10.4049/jimmunol.1600875. Epub 2016 Dec 16. PMID: 27986910

19. Sachs K, Perez O, Pe'er D, Lauffenburger DA, Nolan GP. Causal protein-signaling networks derived from multiparameter single-cell data. Science. 308(5721):523-9. Erratum in: Science. 2005 Aug 19;309(5738):1187. PMID: 15845847

20. Pe'er D. 2005. Bayesian network analysis of signaling networks: a primer. Sci STKE. 2005 Apr 26;2005(281):pl4. Review. PMID: 15855409

21. Werhli AV. 2012. Comparing the reconstruction of regulatory pathways with distinct Bayesian networks inference methods. Werhli AV. BMC Genomics. 13 Suppl 5:S2. doi: 10.1186/1471-2164-13-S5-S2. Epub 2012 Oct 19. PMID: 23095805 Free PMC Article

22. Grzegorczyk M. 2010. An introduction to Gaussian Bayesian networks. Methods Mol Biol. 662:121-47. doi: 10.1007/978-1-60761-800-3_6. PMID: 20824469

23. Koch M, Broom BM, Subramanian D. 2009. Learning robust cell signalling models from high throughput proteomic data. Int J Bioinform Res Appl. 5(3):241-53. PMID: 19525198

24. Ferlay J, Colombet M, Soerjomataram I, Mathers C, Parkin DM, Piñeros M, Znaor A, Bray F. 2019. Estimating the global cancer incidence and mortality in 2018: GLOBOCAN sources and methods. Int J Cancer. 144(8):1941-1953. doi: 10.1002/ijc.31937. Epub 2018 Dec 6. PMID: 30350310

25. Chuang J, Chao J, Hendifar A, Klempner SJ, Gong J. 2019. Checkpoint inhibition in advanced gastroesophageal cancer: clinical trial data, molecular subtyping, predictive biomarkers, and the potential

of combination therapies. Transl Gastroenterol Hepatol. 2019 Aug 27;4:63. doi: 10.21037/tgh.2019.08.04. eCollection 2019. Review. PMID: 31559344

26. Gogoshin G, Boerwinkle E, Rodin AS. 2017. New algorithm and software (BNOmics) for inferring and visualizing Bayesian networks from heterogeneous “big” biological and genetic data. J Comput Biol 23:1–17

27. Andrews B, Ramsey J, Cooper GF. 2018. Scoring Bayesian Networks of Mixed Variables. Int J Data Sci Anal. 2018 Aug;6(1):3-18. doi: 10.1007/s41060-017-0085-7. Epub 2018 Jan 11. PMID: 30140730

28. Zhang X, Branciamore S, Gogoshin G, Rodin AS, Riggs AD. 2017. Analysis of high-resolution 3D intrachromosomal interactions aided by Bayesian network modeling. Proc Natl Acad Sci U S A. 114(48): E10359-E10368. doi: 10.1073/pnas.1620425114. Epub 2017 Nov 13. PMID: 29133398

29. Guyon, E., and A. Elisseeff. 2003. An Introduction to Variable and Feature Selection. Journal of Machine Learning Research 3:1157-1182

S1 Appendix: Bayesian networks obtained from the remaining sub-datasets in the present study (i.e., Adaptive immune signaling network panel x Non-naïve CD4 sub-dataset, and both Adaptive and Checkpoint panels x Naïve CD4, Naïve CD8 and Non-naïve CD8 sub-datasets).

S1 Figures 1-9 - Checkpoint, Naïve CD4;

S1 Figures 10-18 – Checkpoint, Non-naïve CD8;

S1 Figures 19-27 – Checkpoint, Naïve CD8;

S1 Figures 28-36 – Adaptive, Non-naïve CD4;

S1 Figures 37-45 – Adaptive, Naïve CD4;

S1 Figures 46-54 – Adaptive, Non-naïve CD8;

S1 Figures 55-63 – Adaptive, Naïve CD8.

Within each group, the nine networks are as follows:

Day 1, responders

Day 1, non-responders

Day 21, responders,

Day 21, non-responders,

Day 1 and day 21, responders, with “day” contrast variable,

Day 1 and day 21, non-responders, with “day” contrast variable,

Day 1, responders and non-responders, with “response” contrast variable,

Day 21, responders and non-responders, with “response” contrast variable,

“Supergraph” (all data pooled together, with a four-state “contrast” variable).

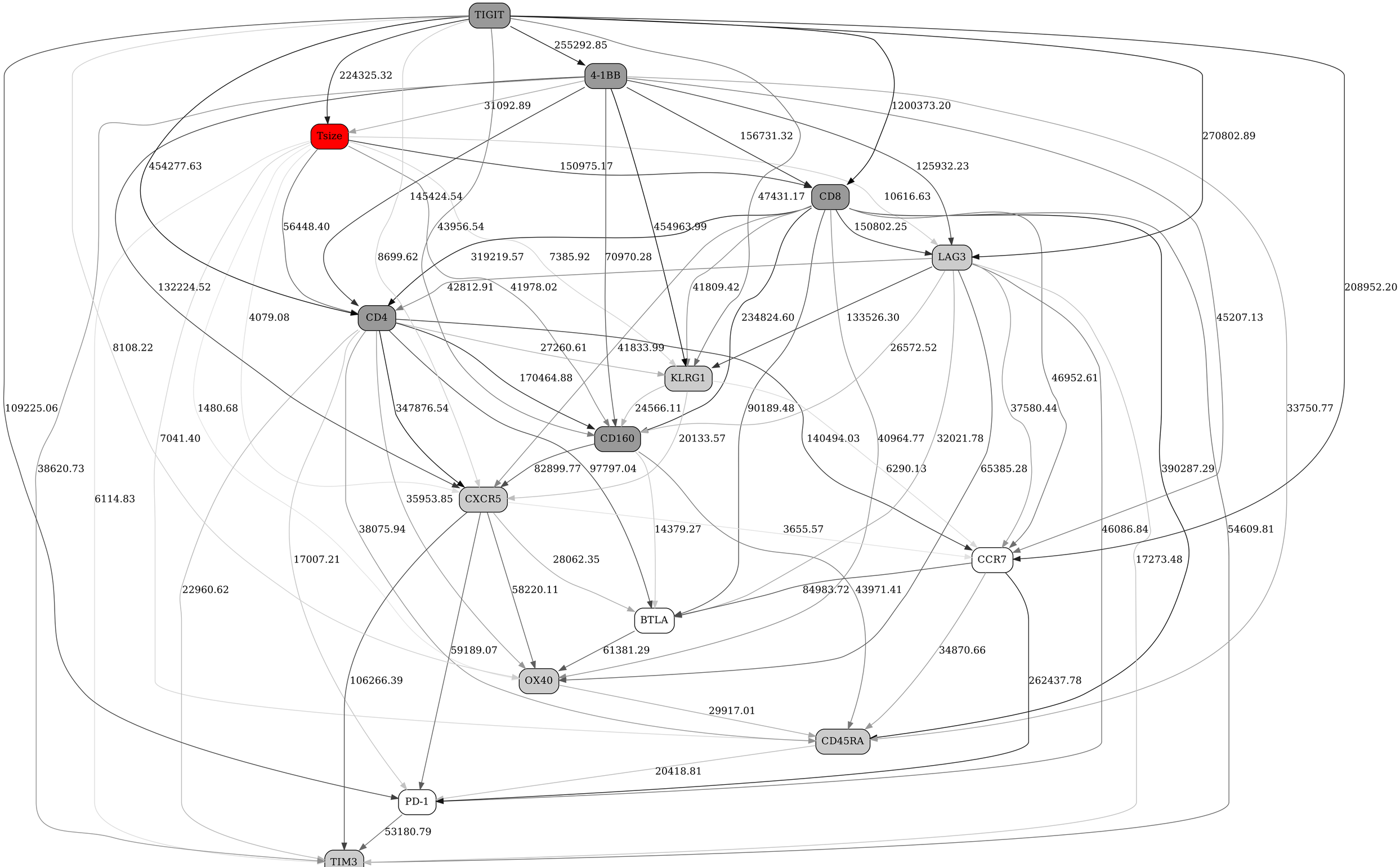
TIGIT
4-1BB
Tsize
CD8
LAG3
CD4
KLRG1
CD160
CXCR5
CCR7
BTLA
OX40
CD45RA
PD-1
TIM3
255292.85
224325.32
31092.89
1200373.20
156731.32
270802.89
454277.63
150975.17
125932.23
145424.54
47431.17
10616.63
56448.40
43956.54
454963.99
150802.25
8699.62
319219.57
7385.92
70970.28
132224.52
42812.91
41978.02
41809.42
208952.20
4079.08
234824.60
133526.30
45207.13
8108.22
27260.61
41833.99
26572.52
170464.88
46952.61
109225.06
1480.68
347876.54
24566.11
90189.48
37580.44
33750.77
7041.40
20133.57
140494.03
40964.77
32021.78
38620.73
82899.77
97797.04
6290.13
65385.28
390287.29
6114.83
35953.85
38075.94
14379.27
3655.57
46086.84
54609.81
17007.21
28062.35
17273.48
22960.62
58220.11
84983.72
43971.41
59189.07
61381.29
34870.66
106266.39
262437.78
29917.01
20418.81
53180.79

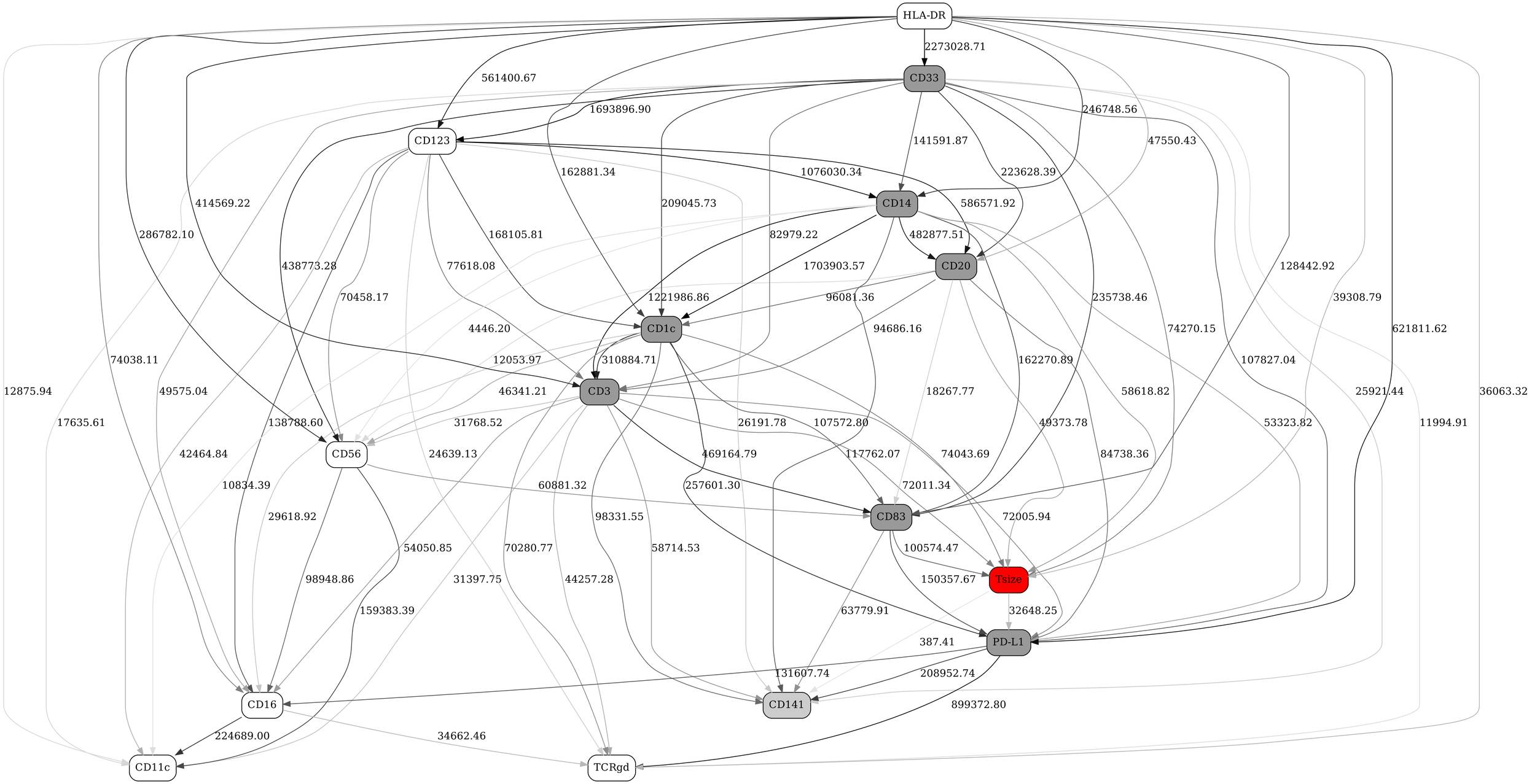
HLA-DR
2273028.71
CD33
561400.67
1693896.90
246748.56
CD123
141591.87
47550.43
162881.34
1076030.34
223628.39
CD14
414569.22
209045.73
586571.92
286782.10
168105.81
82979.22
482877.51
CD20
438773.28
77618.08
1703903.57
128442.92
70458.17
1221986.86
96081.36
235738.46
39308.79
4446.20
CD1c
94686.16
74270.15
621811.62
74038.11
12053.97
310884.71
162270.89
107827.04
12875.94
49575.04
46341.21
CD3
18267.77
58618.82
25921.44
36063.32
17635.61
138788.60
31768.52
26191.78
107572.80
49373.78
53323.82
11994.91
42464.84
CD56
24639.13
469164.79
117762.07
74043.69
84738.36
10834.39
60881.32
257601.30
72011.34
29618.92
98331.55
CD83
72005.94
54050.85
70280.77
58714.53
100574.47
98948.86
31397.75
44257.28
150357.67
Tsize
159383.39
63779.91
32648.25
387.41
PD-L1
131607.74
208952.74
CD16
CD141
899372.80
224689.00
34662.46
CD11c
TCRgd

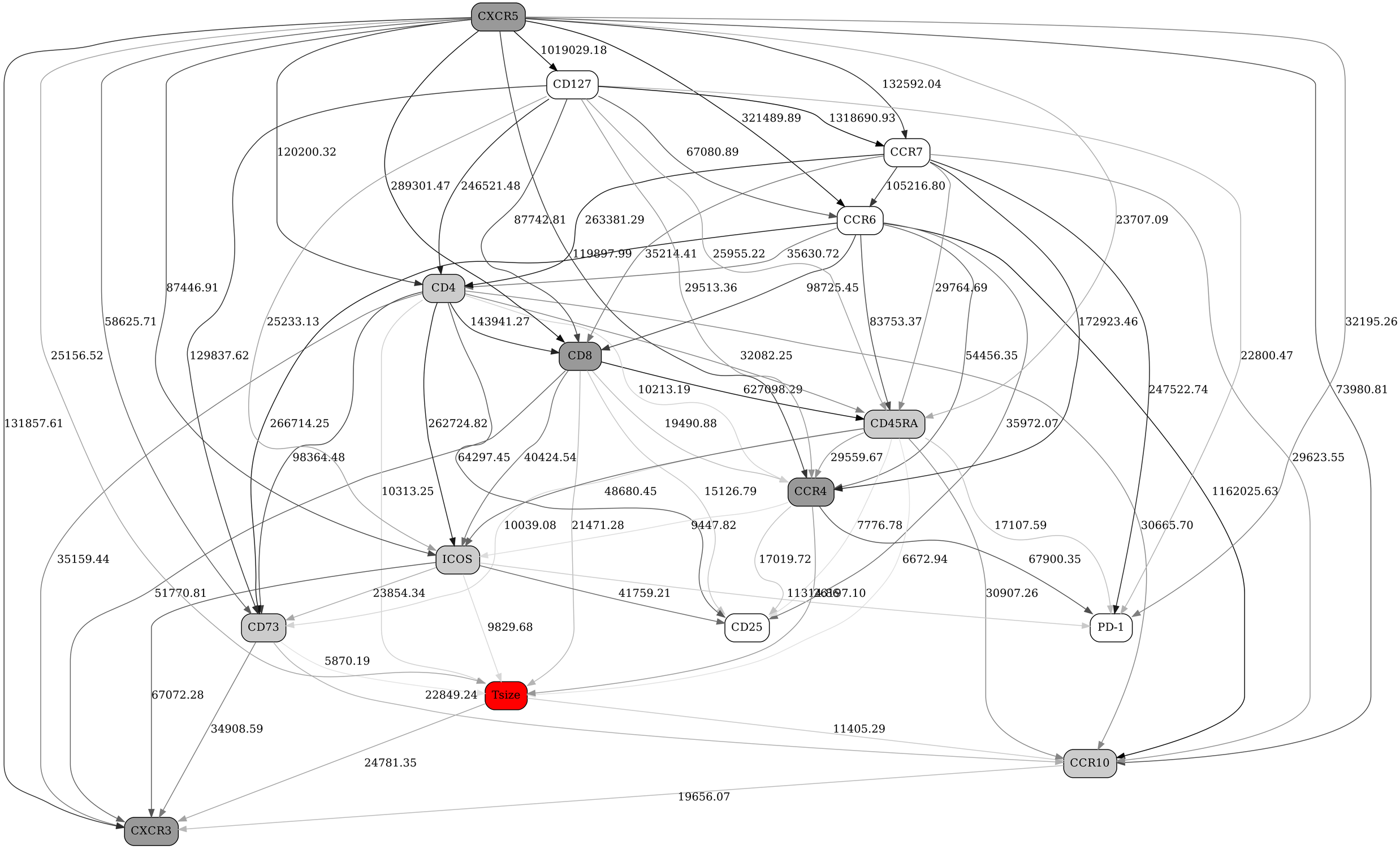
CXCR5
CD127
CCR7
CCR6
CD4
CD8
CD45RA
CCR4
ICOS
CD73
CD25
PD-1
Tsize
CCR10
CXCR3
1019029.18
132592.04
321489.89
1318690.93
120200.32
67080.89
289301.47
246521.48
105216.80
87742.81
263381.29
23707.09
119897.99
35214.41
25955.22
35630.72
87446.91
29513.36
98725.45
29764.69
58625.71
25233.13
143941.27
83753.37
172923.46
32195.26
25156.52
129837.62
32082.25
54456.35
22800.47
10213.19
627098.29
247522.74
73980.81
131857.61
266714.25
262724.82
19490.88
35972.07
98364.48
64297.45
40424.54
29559.67
29623.55
10313.25
48680.45
15126.79
1162025.63
10039.08
21471.28
9447.82
7776.78
17107.59
30665.70
35159.44
17019.72
6672.94
67900.35
51770.81
23854.34
41759.21
30907.26
9829.68
5870.19
67072.28
22849.24
34908.59
11405.29
24781.35
19656.07

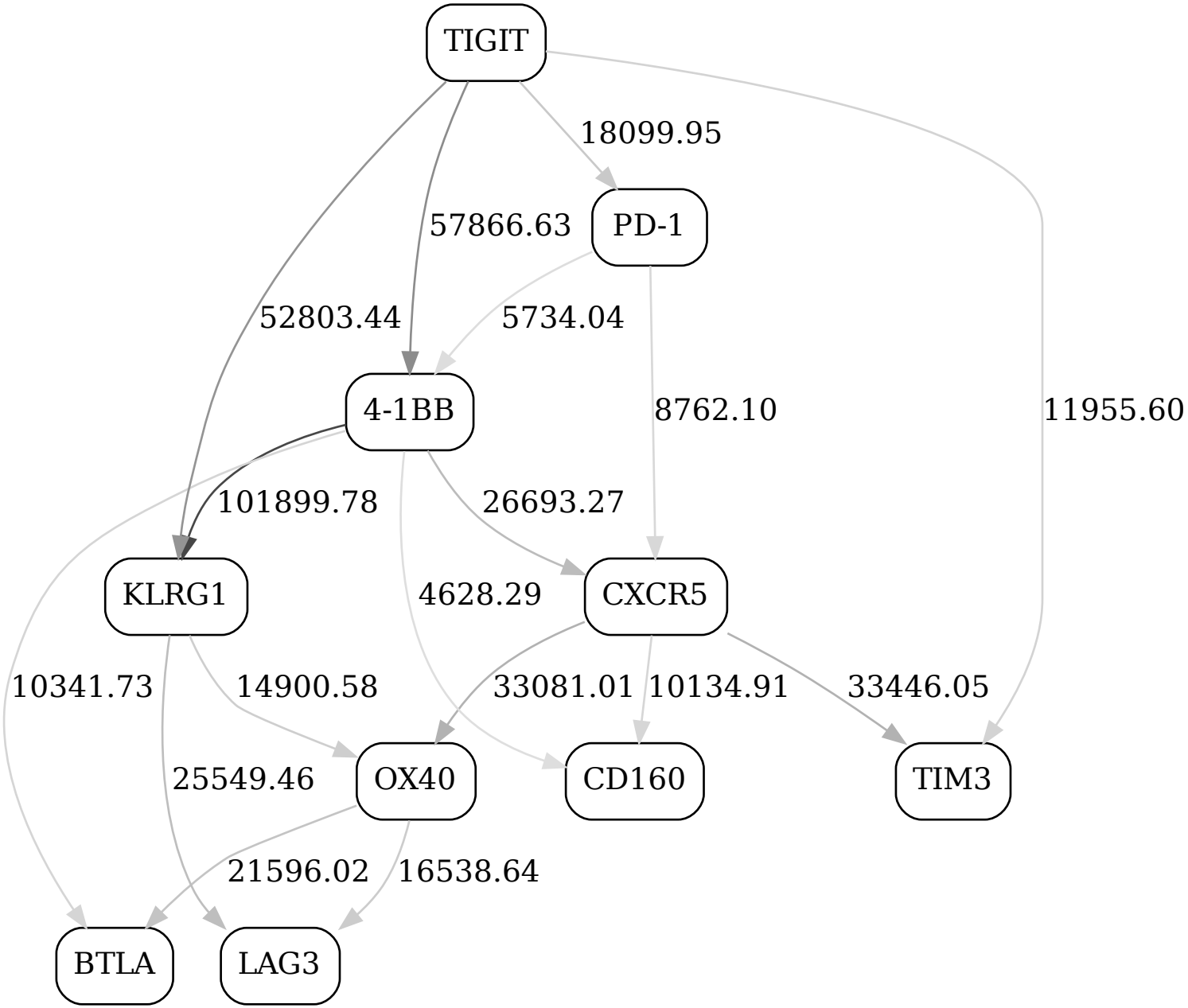
TIGIT
18099.95
PD-1
57866.63
52803.44
5734.04
4-1BB
8762.10
11955.60
101899.78
26693.27
KLRG1
4628.29
CXCR5
10341.73
14900.58
33081.01
10134.91
33446.05
25549.46
OX40
CD160
TIM3
21596.02
16538.64
BTLA
LAG3

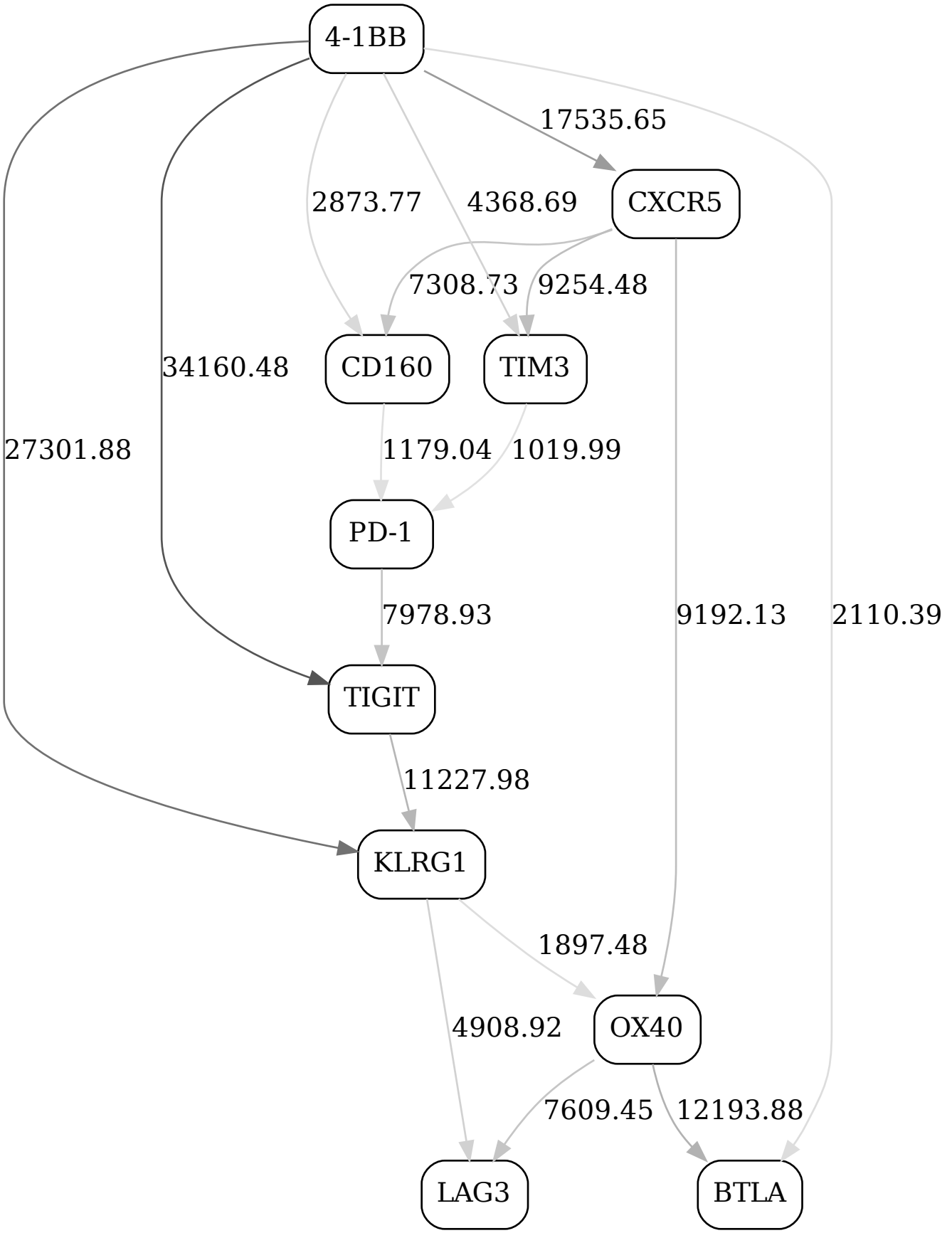
4-1BB
17535.65
CXCR5
2873.77
4368.69
7308.73
9254.48
CD160
TIM3
34160.48
27301.88
1179.04
1019.99
PD-1
7978.93
9192.13
2110.39
TIGIT
11227.98
KLRG1
1897.48
4908.92
OX40
7609.45
12193.88
LAG3
BTLA

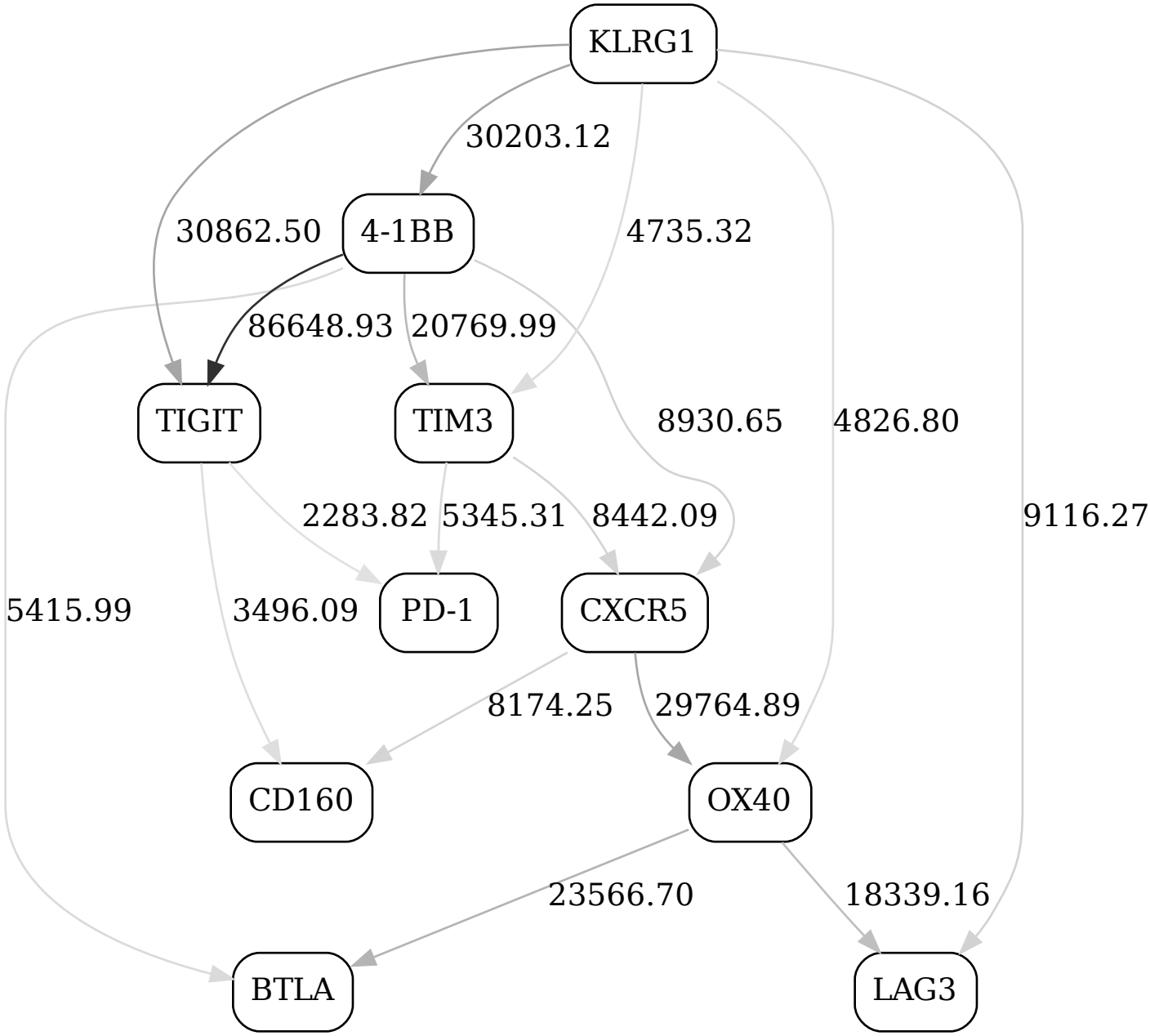
KLRG1
30203.12
30862.50
4-1BB
4735.32
86648.93
20769.99
TIGIT
TIM3
8930.65
4826.80
2283.82
5345.31
8442.09
9116.27
5415.99
3496.09
PD-1
CXCR5
8174.25
29764.89
CD160
OX40
23566.70
18339.16
BTLA
LAG3

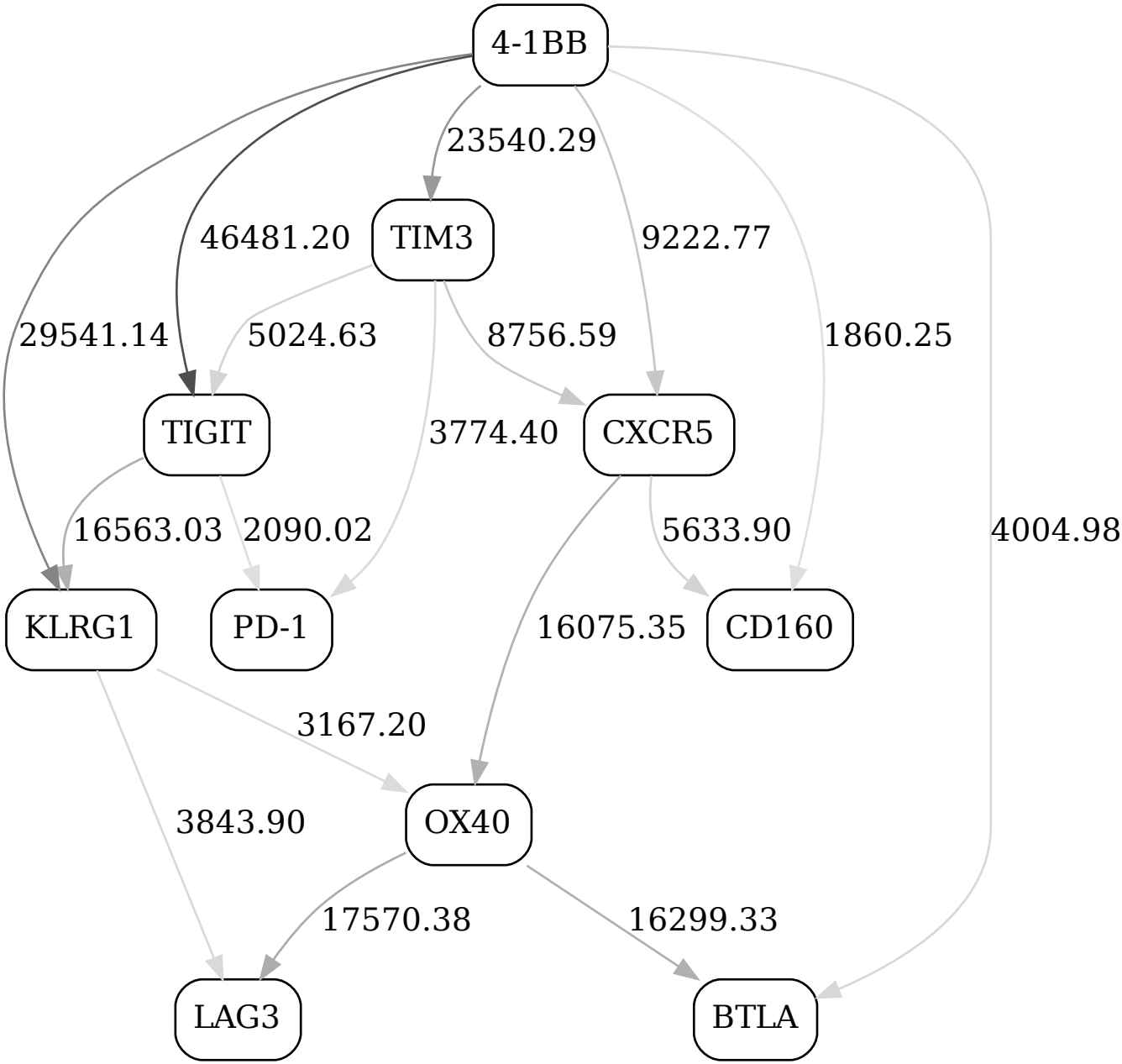
4-1BB
23540.29
TIM3
46481.20
9222.77
29541.14
5024.63
8756.59
1860.25
TIGIT
3774.40
CXCR5
16563.03
2090.02
5633.90
4004.98
KLRG1
PD-1
16075.35
CD160
3167.20
3843.90
OX40
17570.38
16299.33
LAG3
BTLA

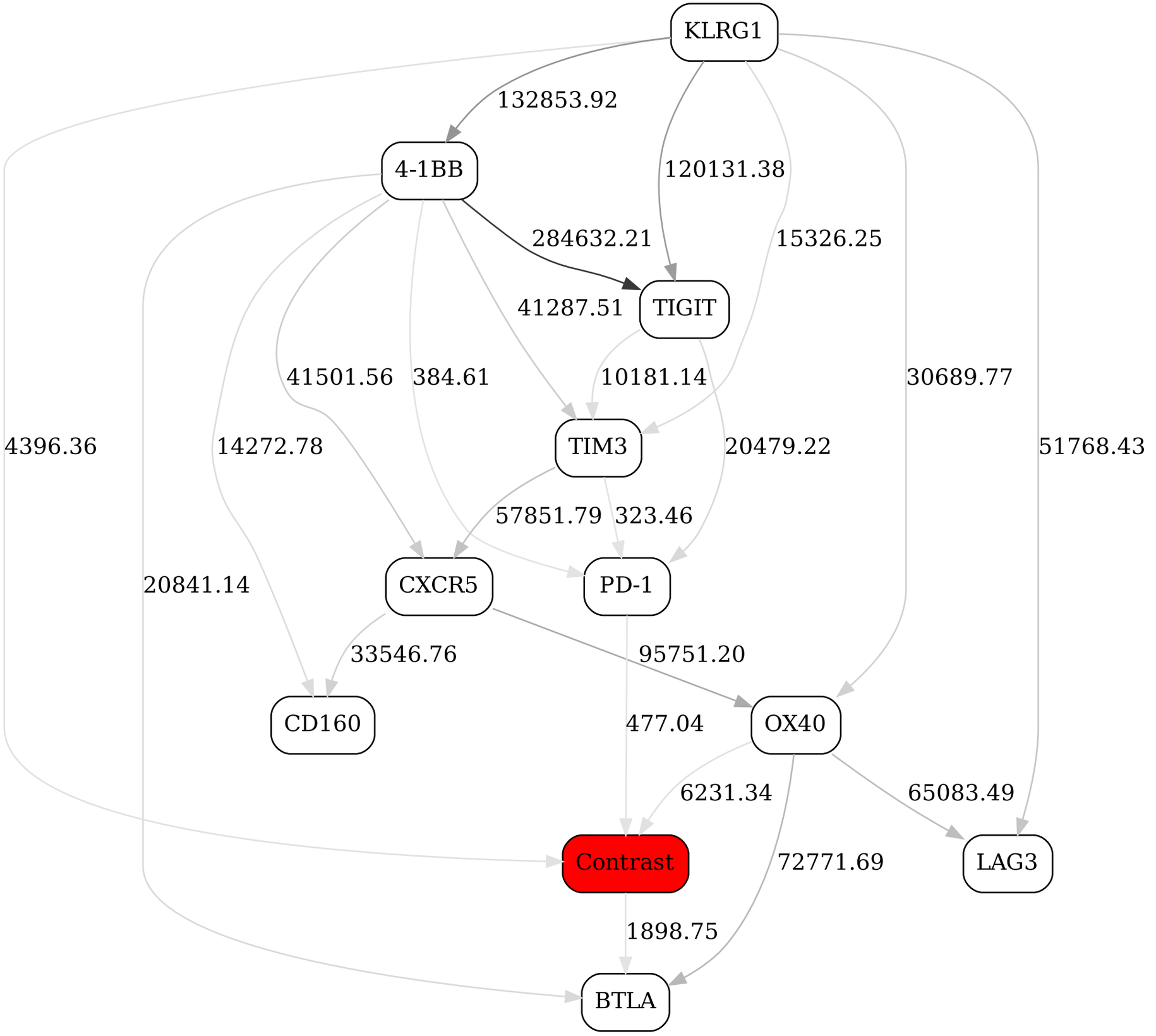
KLRG1
132853.92
4-1BB
120131.38
284632.21
15326.25
41287.51
TIGIT
41501.56
384.61
10181.14
30689.77
4396.36
14272.78
TIM3
20479.22
51768.43
57851.79
323.46
20841.14
CXCR5
PD-1
33546.76
95751.20
CD160
477.04
OX40
6231.34
65083.49
Contrast
72771.69
LAG3
1898.75
BTLA

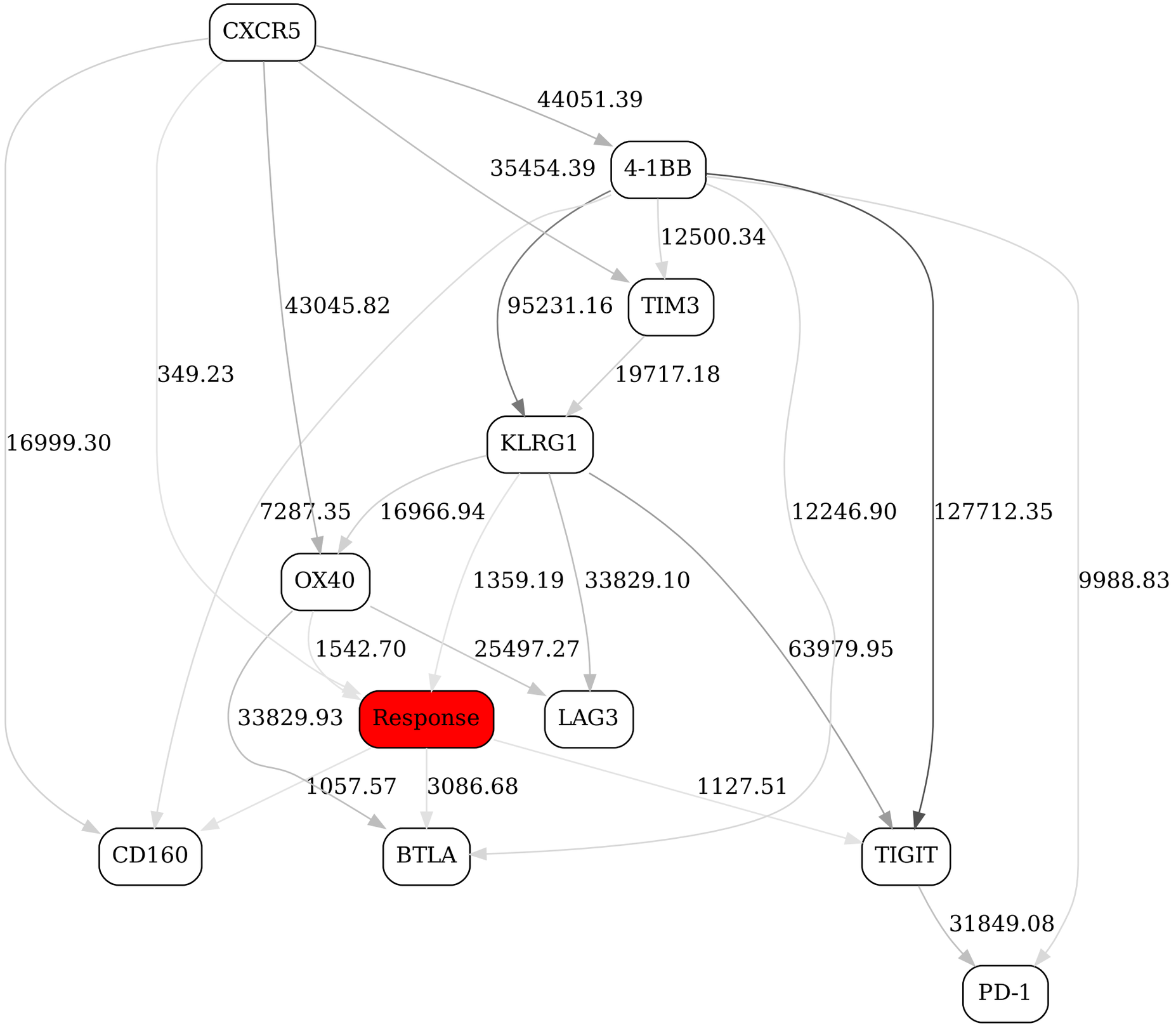
CXCR5
44051.39
35454.39
4-1BB
12500.34
43045.82
95231.16
TIM3
349.23
19717.18
16999.30
KLRG1
7287.35
16966.94
12246.90
127712.35
OX40
1359.19
33829.10
9988.83
1542.70
25497.27
63979.95
33829.93
Response
LAG3
1057.57
3086.68
1127.51
CD160
BTLA
TIGIT
31849.08
PD-1

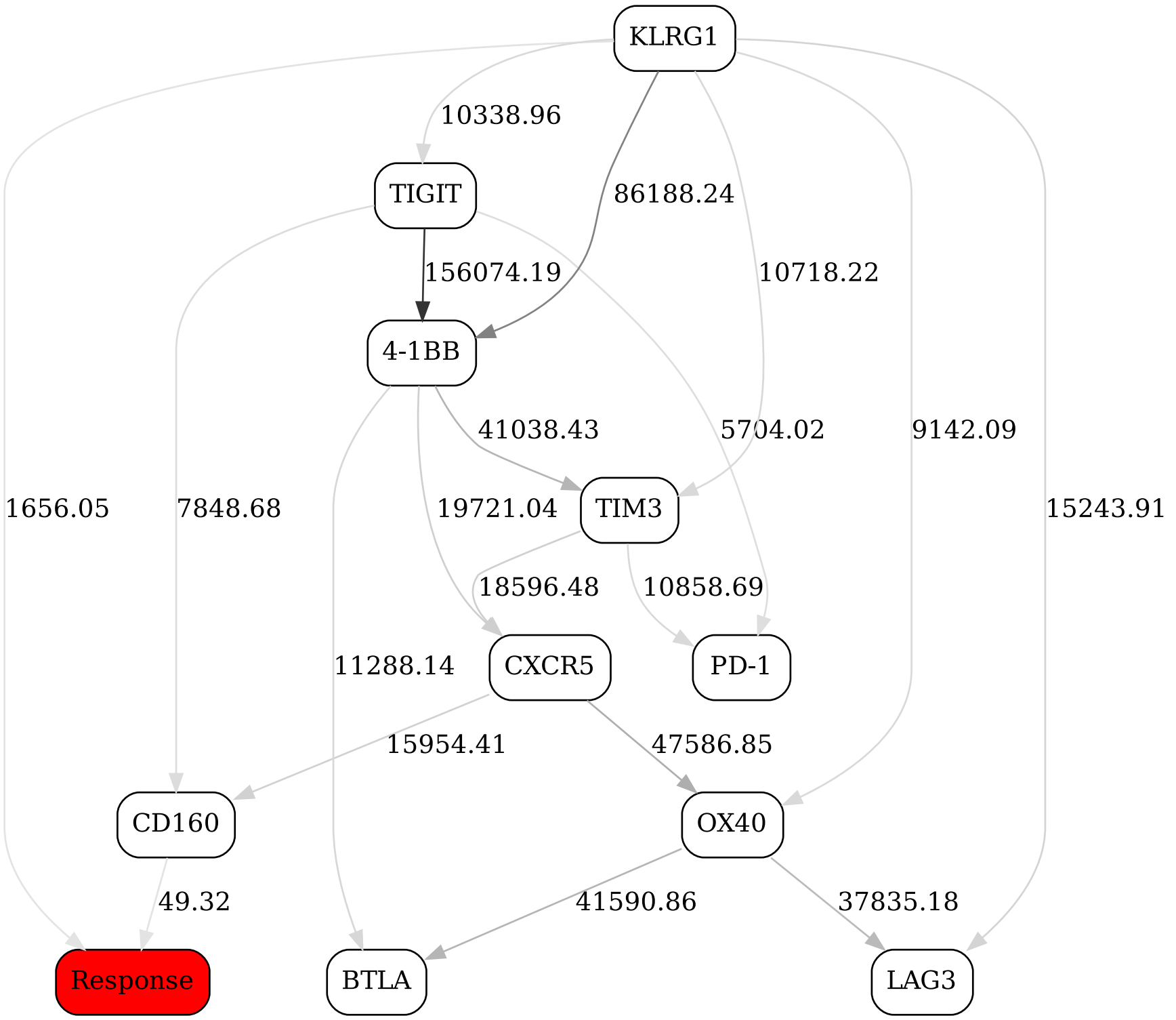
KLRG1
10338.96
TIGIT
86188.24
156074.19
10718.22
4-1BB
41038.43
5704.02
9142.09
1656.05
7848.68
19721.04
TIM3
15243.91
18596.48
10858.69
11288.14
CXCR5
PD-1
15954.41
47586.85
CD160
OX40
49.32
41590.86
37835.18
Response
BTLA
LAG3

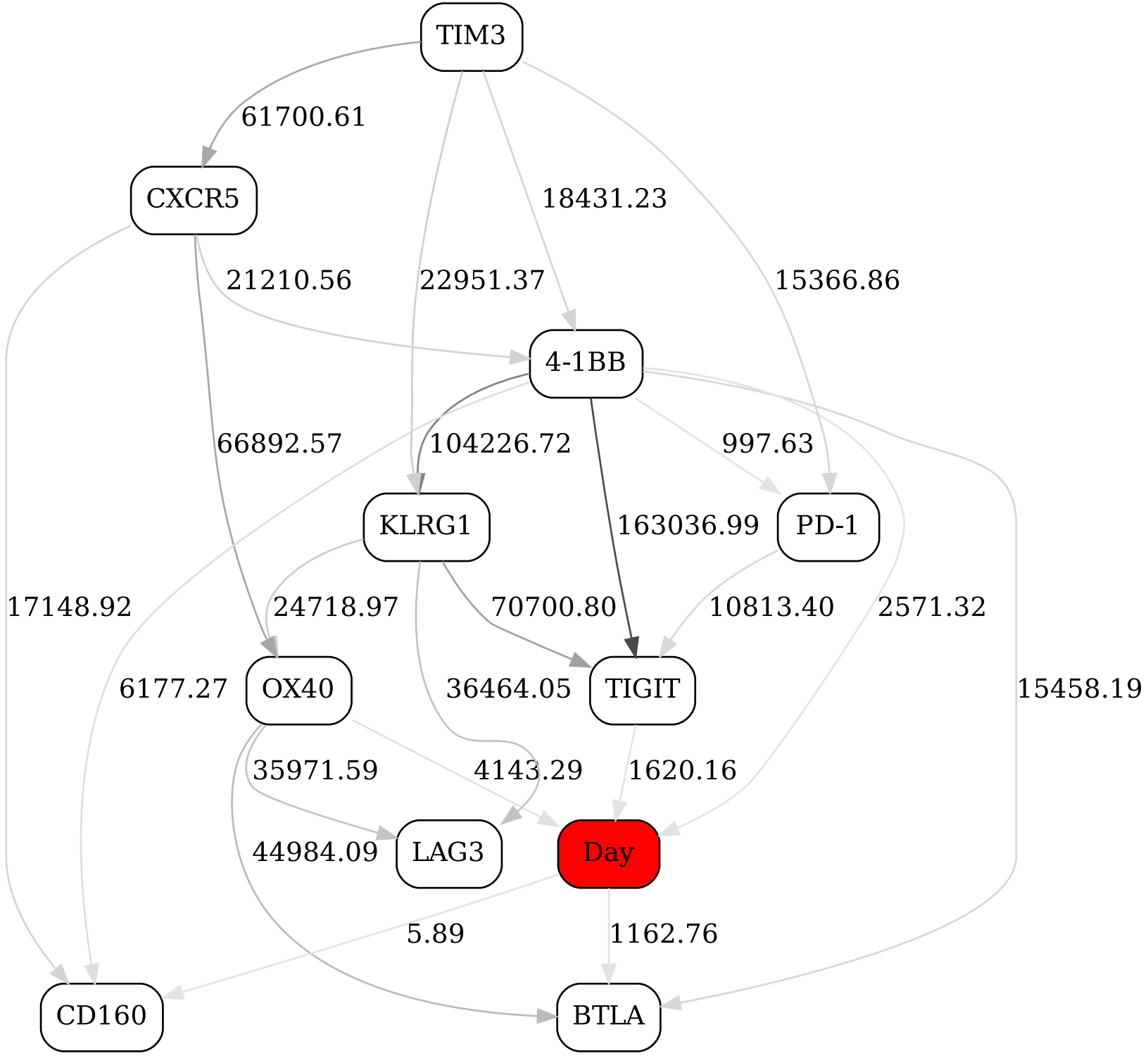
TIM3
61700.61
CXCR5
18431.23
21210.56
22951.37
15366.86
4-1BB
66892.57
104226.72
997.63
KLRG1
163036.99
PD-1
17148.92
24718.97
70700.80
10813.40
2571.32
6177.27
OX40
36464.05
TIGIT
15458.19
35971.59
4143.29
1620.16
44984.09
LAG3
Day
5.89
1162.76
CD160
BTLA

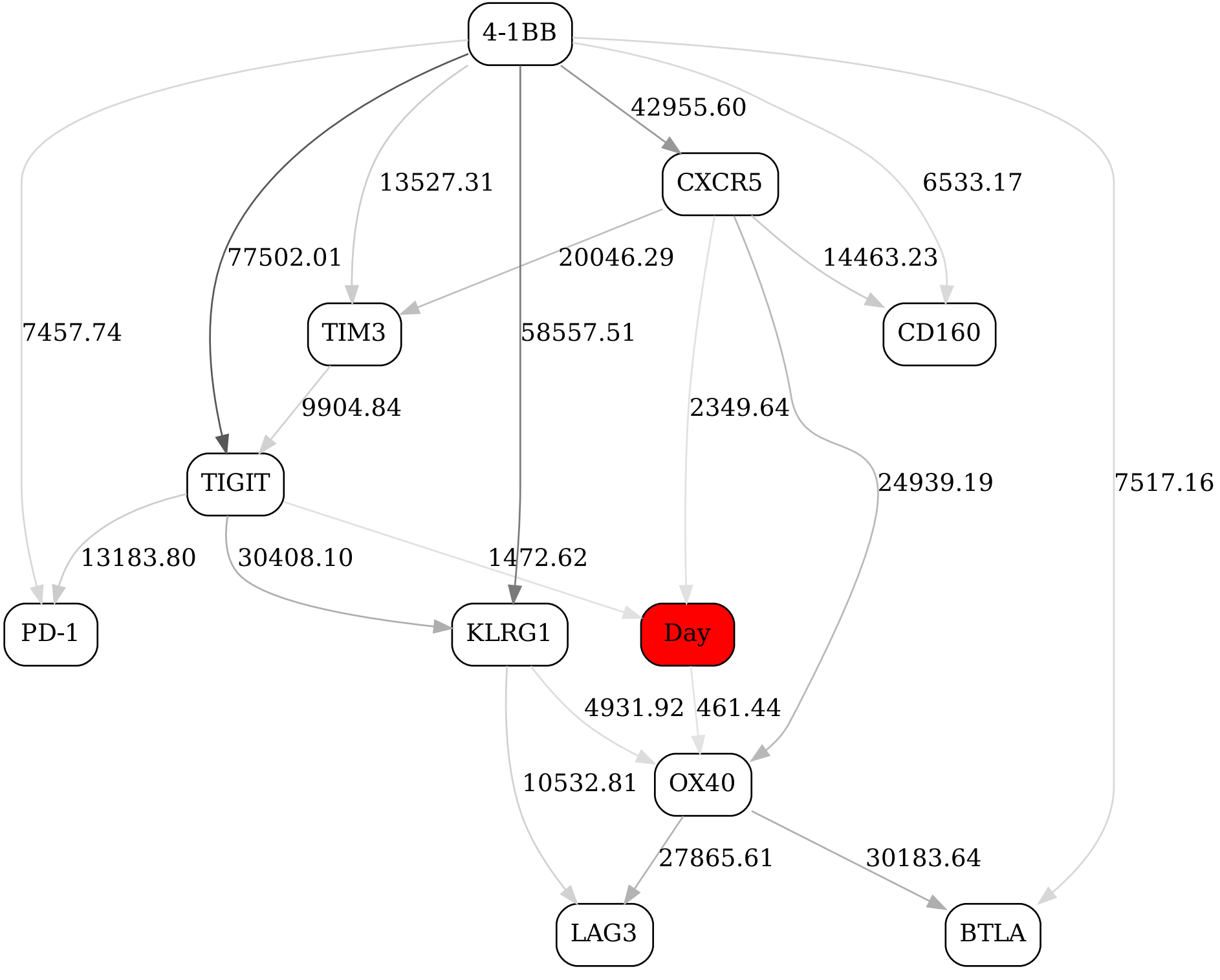
4-1BB
42955.60
CXCR5
13527.31
6533.17
77502.01
20046.29
14463.23
7457.74
TIM3
58557.51
CD160
9904.84
2349.64
TIGIT
24939.19
7517.16
13183.80
30408.10
1472.62
PD-1
KLRG1
Day
4931.92
461.44
10532.81
OX40
27865.61
30183.64
LAG3
BTLA